CHEMISTRY OF MATERIALS
Article

Chem. Mater. **2010,** *22,* 3043–3050 3043
DOI:10.1021/cm903727u

Hydrothermal Synthesis of Monoclinic VO_2 Micro- and Nanocrystals in One Step and Their Use in Fabricating Inverse Opals

Jung-Ho Son,*[,†,‡] Jiang Wei,[§] David Cobden,[§] Guozhong Cao,[‡] and Younan Xia[†,⊥]

[†]*Department of Chemistry,* [‡]*Department of Materials Science and Engineering, and* [§]*Department of Physics, University of Washington, Seattle, Washington 98195, and* [⊥]*Department of Biomedical Engineering, Washington University, St. Louis, Missouri 63130*

Received December 14, 2009. Revised Manuscript Received March 31, 2010

Monoclinic vanadium dioxide VO_2(M) shows a reversible first-order metal−insulator transition (MIT) to metallic rutile phase VO_2(R) at a temperature of T_c = ∼68 °C. Synthesis of micro- and nanocrystals of VO_2(M) by a direct one-step hydrothermal method is reported herein. The reaction employs a combination of a hydrolyzed precipitate of VO^{2+} with hydrazine and NaOH. The morphology and composition of the product depends on the conditions used for preparing the precursor, including pH, temperature, and NaOH concentration. Asterisk or rod shaped VO_2(M) microcrystals or hexagon shaped nanocrystals were obtained depending on the reaction conditions, admixed with VO_2(B) nanowires. Higher temperature, pH or NaOH concentration during the precursor formation favored VO_2(M) and VO_2(B) nanocrystals. The VO_2(M) microcrystals showed the expected metal−insulator transition at around 67 °C which was monitored by optical microscopy. As a demonstration of their potential use, we used the VO_2 nanocrystals to infiltrate opaline lattices of polystyrene beads to generate inverse opals.

Introduction

Monoclinic vanadium dioxide VO_2(M) shows a reversible first-order metal−insulator transition (MIT) at a temperature of T_c = ∼68 °C. On warming through the transition, drastic changes occur in both electrical and optical properties[1,2] as the insulating monoclinic form VO_2(M) converts to the metallic rutile form VO_2(R).[3,4] As a result, the material has been considered for applications in field-effect transistors,[5,6] switches,[7−9] sensors,[10,11] and smart windows.[12,13] However, because of stresses due to the change in shape of the unit cell and the latent heat, the material exhibits hysteresis in its properties and mechanical degradation on passing through the phase transition.[14]

Nanoscale VO_2(M) crystals offer the possibility of avoiding these problems and obtaining a sharper, more reproducible transition.[15] Recently VO_2(M) nanobeams have been grown by physical vapor deposition on amorphous substrates at high temperatures and low pressures.[16,17] In these samples, the MIT was sharp and reproducible, and tungsten doping was successfully used to reduce the transition temperature.[18,19] However, direct low-temperature solution synthesis of nanoscale VO_2(M), which would allow it to be used for applications in large quantities, has proved challenging although VO_2(M) is the thermodynamically stable phase. To date, low temperature hydrothermal reactions in solution have mostly yielded nanowires or

*To whom correspondence should be addressed. E-mail: jhson@u.washington.edu.

(1) Morin, F. J. *Phys. Rev. Lett.* **1959**, *3*, 34.
(2) Zylbersztejn, A.; Mott, N. F. *Phys. Rev. B* **1975**, *11*, 4383.
(3) Marezio, M.; McWhan, B.; Dernier, P. D.; Remeika, J. P. *Phys. Rev. B* **1972**, *5*, 2541.
(4) Cavalleri, A.; Dekorsy, T.; Chong, H. H. W.; Kieffer, J. C.; Schoenlein, R. W. *Phys. Rev. B* **2004**, *70*, 161102/1.
(5) Kim, H.-T.; Chae, B.-G.; Youn, D.-H.; Maeng, S.-L.; Kim, G.; Kang, K.-Y.; Lim, Y.-S. *New J. Phys.* **2004**, *6*, 52.
(6) Chen, C.; Zhou, Z. *Appl. Phys. Lett.* **2007**, *91*, 011107/1.
(7) Saitzek, S.; Guirleo, G.; Guinneton, F.; Sauques, L.; Villain, S.; Aguir, K.; Leroux, C.; Gavarri, J.-R. *Thin Solid Films* **2004**, *449*, 166.
(8) Partlow, D. P.; Gurkovich, S. R.; Radford, K. C.; Denes, L. J. *J. Appl. Phys.* **1991**, *70*, 443.
(9) Soltani, M.; Chaker, M.; Haddad, E.; Kruzelesky, R. *Meas. Sci. Technol.* **2006**, *17*, 1052.
(10) Kim, B. J.; Lee, Y. W.; Chae, B. G.; Yun, S. J.; Oh, S. Y.; Kim, H. T.; Lim, Y. S. *Appl. Phys. Lett.* **2007**, *90*, 023515/1.
(11) Liu, H.; Rua, A.; Vasquez, O.; Vikhnin, V. S.; Fernandez, F. E.; Fonseca, L. F.; Resto, O.; Weisz, S. Z. *Sensors* **2005**, *5*, 185.
(12) Babulanam, S. M.; Eriksson, T. S.; Niklasson, G. A.; Granqvist, C. G. *Solar Energy Mater.* **1987**, *16*, 347.
(13) Manning, T. D.; Parkin, I. P.; Pemble, M. E.; Sheel, D.; Vernardou, D. *Chem. Mater.* **2004**, *16*, 744.
(14) Kim, H. K.; You, H.; Chiarello, R. P.; Chang, H. L. M.; Zhang, T. J.; Lam, D. J. *Phys. Rev. B* **1993**, *47*, 12900.
(15) Suh, J. Y.; Lopez, R.; Feldman, L. C.; Haglund, R. F., Jr. *J. Appl. Phys.* **2004**, *96*, 1209.
(16) Guiton, B. S.; Gu, Q.; Prieto, A. L.; Gudiksen, M. S.; Park, H. *J. Am. Chem. Soc.* **2005**, *127*, 498.
(17) Sohn, J. I.; Joo, H. J.; Porter, A. E.; Choi, C.-J.; Kim, K.; Kang, D. J.; Welland, M. E. *Nano Lett.* **2007**, *7*, 1570.
(18) Wu, J. Q.; Gu, Q.; Guiton, B. S.; de Leon, N. P.; Lian, O. Y.; Park, H. *Nano Lett.* **2006**, *6*, 2313.
(19) Gu, Q.; Falk, A.; Wu, J. Q.; Lian, O. Y.; Park, H. *Nano Lett.* **2007**, *7*, 363.
(20) Chen, W.; Peng, J.; Mai, L.; Yu, H.; Qi, Y. *Solid State Commun.* **2004**, *132*, 513.
(21) Chen, X.; Wang, X.; Wang, Z.; Wan, J.; Liu, J.; Qian, Y. *Nanotechnology* **2004**, *15*, 1685.
(22) Liu, J. F.; Li, Q. H.; Wang, T. H.; Yu, D. P.; Li, Y. D. *Angew. Chem., Int. Ed.* **2004**, *43*, 5048.
(23) Mai, L.; Chen, W.; Xu, Q.; Peng, J.; Zhu, Q. *Int. J. Nanoscience* **2004**, *3*, 225.
(24) Pavasupree, S.; Suzuki, Y.; Kitiyanan, A.; Pivsa-Art, S.; Yoshikawa, S. *J. Solid State Chem.* **2005**, *178*, 2152.

Published on Web 04/19/2010

nanorods of the metastable VO_2(B) phase.[20−25] VO_2(B) could be transformed to VO_2(M) by heat treatment[26−31] or phase transformation reaction in solution,[32] but to our knowledge, there have been only a few reports of one-step synthesis of VO_2(M) in a low-temperature solution reaction prior to the recently reported methods of hydrothermal treatment of V_2O_4 in alcohol[33] and hydrothermal reaction of V_2O_5 with oxalic acid.[34,35] In this paper, we report hydrothermal synthesis and characterization of VO_2(M) micro- and nanocrystals by hydrothermal treatment of hydrolyzed precipitate from V_2O_5 using N_2H_4 as a reducing agent. The dependence of morphology on the reaction conditions and VO_2 inverse opal fabrication using VO_2 nanocrystals are also described herein.

Experimental Section

Synthesis of VO_2 Micro- and Nanocrystals. In a typical reaction, V_2O_5 (Alfa Aesar, 0.45 g) was first stirred with 10 mL of deionized water to make a yellow suspension. Then 0.75 mL of H_2SO_4 (Fisher Scientific) was added to the suspension while heating at around 60 °C. 0.25 mL of hydrazine hydrate (Aldrich, 99%) was added dropwise to the solution. The solution turned green and then blue, indicating the reduction of V^{5+} to V^{4+}. Alternatively, $VOSO_4$ (Aldrich, 97%) was used instead of a mixture of V_2O_5 and H_2SO_4. In this case, hydrazine was still necessary for the formation of VO_2(M). The pH of the resultant strongly acidic blue VO^{2+} solution was then adjusted to between 4 and 10 by adding NaOH solution. Heat could also be applied to the solution while adding NaOH solution. A gray to brown precipitate formed during the addition of NaOH solution. The precipitate was filtered and washed with water. The filtered precipitate was collected without drying, and then dispersed in 10 mL of water. Hydrothermal reaction was carried out in a Teflon-lined autoclave with a capacity of 23 mL at 220 °C for 48 h. The final black product was separated by filtration or centrifugation, followed by washing with water and ethanol.

Polystyrene Colloidal Crystal. Polystyrene (PS) beads with a diameter of 500 nm (Polyscience) were used as a colloidal crystal template. A previously reported vertical evaporation method was used to obtain a PS colloidal crystal on a substrate,[36] which is briefly described as follows: A slide glass was cleaned with detergent and rinsed with water and ethanol. After drying, the glass was treated in a plasma cleaner to make its surface hydrophilic. The original commercial PS bead dispersion was diluted to 0.1 wt % concentration in deionized water. The cleaned slide glass was then vertically dipped in the prepared PS solution, and the container was placed in an oven at 60 °C until the solution was completely evaporated. A closely packed PS colloidal crystal formed on the glass substrate as a result, giving the film a bright iridescent appearance.

VO_2 Nanocrystal Infiltration. VO_2 nanocrystals originally dispersed in aqueous reaction solution were transferred to ethanol by several centrifuge-redispersion cycles with deionized water and ethanol. The ethanolic dispersion of VO_2 nanocrystals was then diluted for VO_2 nanocrystal infiltration. The infiltration procedure was similar to the way the PS colloidal crystal was formed. A piece of PS colloidal crystal glass substrate cut into 2 cm ×0.5 cm was held vertically in a small vial filled with the ethanolic dispersion of VO_2 nanocrystals. The solution was evaporated in an oven at 60 °C. Parts of colloidal crystal successfully infiltrated with VO_2 had a weak iridescent black appearance.

Removal of PS Template. The PS colloidal crystal infiltrated with VO_2 nanocrystals was calcined in a tube furnace under N_2 flowing at 500 °C for 2 h. The resultant black inverse opal VO_2 film showed weak iridescence. Alternatively, toluene was used to remove the PS template instead of calcination. After treatment with toluene, the substrate was calcined at 500 °C for 2 h under N_2 to ensure the removal of the PS template.

Instruments. X-ray diffraction (XRD) was measured using a Philips PW-1710 diffractometer with a step size of 0.02°. SEM images were taken using a field emission SEM (Sirion XL, FEI, Hillsboro, OR). The powder sample was directly placed on a carbon tape or dispersed in ethanol and then deposited on a silicon substrate. The sample was coated with a thin layer of Au/Pd in a plasma coater to avoid charging. A Philips EM420 transmission electron microscope was used to obtain TEM images and selected area electron diffraction (SAED) patterns. The TEM sample was prepared by evaporating a diluted dispersion of the product in ethanol on a copper grid coated with holey carbon.

Results and Discussion

Our synthesis started by adding hydrazine and NaOH solution to VO^{2+} solution, producing a gray-brown hydrous precipitate, which is probably a complex of VO^{2+}, OH^-, and hydrazine. XRD of the precipitate revealed that the precipitate was amorphous. The filtered precipitate was easily oxidized, turning green when it was dried, so hydrothermal reaction of the precipitate was carried out without drying.

The overall reaction conditions and product morphologies are summarized in Tables 1−4. The reaction conditions such as pH, concentration, and temperature during the formation of the precipitate were important factors in determining the size and shape of the final product. When the pH was in the range 4−5.5 during precipitate formation, asterisk-shaped VO_2(M) microcrystals or elongated microrods formed. When the pH was higher, VO_2 nanocrystals were preferred. Larger nanocrystals (>100 nm) usually showed a hexagonal plate-like morphology. Increasing the temperature or NaOH concentration during the precipitate formation had a similar effect to the increasing of pH.

Control of Phase and Morphology. Figure 1 shows XRD patterns of the products of four different representative

(25) Sediri, F.; Gharbi, N. *Mater. Sci. Eng., B* **2007**, *139*, 114.
(26) Wu, X.; Tao, Y.; Dong, L.; Wang, Z.; Hu, Z. *Mater. Res. Bull.* **2005**, *40*, 315.
(27) Kam, K. C.; Cheetham, A. K. *Mater. Res. Bull.* **2006**, *41*, 1015.
(28) Zhang, K.-F.; Liu, X.; Su, Z.-X.; Li, H.-L. *Mater. Lett.* **2007**, *61*, 2644.
(29) Whittaker, L.; Zhang, H. S.; Banerjee, S. *J. Mater. Chem.* **2009**, *19*, 2968.
(30) Santulli, A. C.; Xu, W. Q.; Parise, J. B.; Wu, L. S.; Aronson, M. C.; Zhang, F.; Nam, C. Y.; Black, C. T.; Tiano, A. L.; Wong, S. S. *Phys. Chem. Chem. Phys.* **2009**, *11*, 3718.
(31) Xu, C. L.; Ma, X.; Liu, X.; Qiu, W. Y.; Su, Z. X. *Mater. Res. Bull.* **2004**, *39*, 881.
(32) Chen, W.; Mai, L. Q.; Qi, Y. Y.; Dai, Y. *J. Phys. Chem. Solids* **2006**, *67*, 896.
(33) Whittaker, L.; Jaye, C.; Fu, Z.; Fischer, D. A.; Banerjee, S. *J. Am. Chem. Soc.* **2009**, *131*, 8884.
(34) Cao, C.; Gao, Y.; Luo, H. *J. Phys. Chem. C* **2008**, *112*, 18810.
(35) Ji, S.; Zhao, Y.; Zhang, F.; Jin, P. *J. Cryst. Growth* **2010**, *312*, 282.
(36) Jiang, P.; Bertone, J. F.; Hwang, K. S.; Colvin, V. L. *Chem. Mater.* **1999**, *11*, 2132.

Table 1. Reaction Conditions for the Short Asterisk-Shaped Microcrystals

V_2O_5 (g)	H_2SO_4 (ml)	$N_2H_4 \cdot H_2O$ (ml)	temp (°C)[a]	NaOH[a]	pH[b]	ppt[c]	reaction condition	size (μm)	VO_2(M) (%)[d]
0.45	0.75	0.25		1 N	5.5	1/2	220 °C 72 h	1	61
0.9	1.5	0.5		2 g/6 mL	5	1/2	220 °C 48 h	5	81
0.45	0.75	0.25		1 N	5.3		220 °C 48 h	3	56
0.45	0.75	0.25		1 g/3 mL	5.3	1/2	220 °C 48 h	1	77
0.45	0.75	0.25	90	1 N	4 → 2.64		230 °C 48 h	2	100
0.45	0.75	0.25	70	0.9 g	4.1 → 2.6		230 °C 48 h	5	73
0.9	1.5	0.5		2 g/5 mL	5.5 → 2.7	1/2	230 °C 48 h	2	81

[a] Temperature, amount of NaOH, and concentration during preparation of precipitate. [b] The pH after addition of NaOH during preparation of precipitate. The pH after hydrothermal reaction is followed by an arrow. [c] Amount of precipitate used for hydrothermal reaction among the total precipitate formed. [d] Percentage of VO_2(M) among the total product calculated by comparing the intensity of the strongest XRD lines with that of VO_2(B).

Table 2. Reaction Conditions for the Elongated Microrods or Long Asterisk-Shaped Microcrystals

V_2O_5 (g)	H_2SO_4 (ml)	$N_2H_4 \cdot H_2O$ (ml)	temp (°C)[a]	NaOH[a]	pH[b]	ppt[c]	reaction condition	size (μm)	VO_2(M) (%)[d]
0.45	0.75	0.25		1 N	4.5	1/2	220 °C 48 h	3 × 10	75
0.45	0.75	0.25		1 N	5	1/2	220 °C 48 h	3 × 15	83
0.45	0.75	0.25		1 N	5.3		220 °C 48 h	3 × 10	25
0.225	0.375	0.125		0.5 g/3 mL	5.2		220 °C 48 h	2 × 15	77
0.45	0.75	0.25		1 g/10 mL	4.1 → 3.1		230 °C 48 h	2 × 10	
0.225	0.375	0.125	100	1 N 12 mL			220 °C 48 h	2 × 10	58
0.225	0.375	0.125	95	1 N 13 mL	4.5 → 3.5		220 °C 48 h	2 × 10	58

[a] Temperature, amount of NaOH, and concentration during preparation of precipitate. [b] The pH after addition of NaOH during preparation of precipitate. The pH after hydrothermal reaction is after the arrow. [c] Amount of precipitate used for hydrothermal reaction among the total precipitate formed. [d] Percentage of VO_2(M) among the total product calculated by comparing the intensity of the strongest XRD lines with that of VO_2(B).

Table 3. Reaction conditions for the smaller nanocrystals

V_2O_5 (g)	H_2SO_4 (ml)	$N_2H_4 \cdot H_2O$ (ml)	temp (°C)[a]	NaOH[a]	pH[b]	ppt[c]	reaction condition	size (nm)	VO_2(M) (%)[d]
0.45	0.75	0.25	90	1 g/3 mL	4.5		220 °C 48 h	30−60	51
0.225	0.375	0.125	95	1 N 12 mL	5.8 → 7.4		220 °C 48 h	20−100	64
0.225	0.375	0.125	100	1 N 14	11.2 → 7.3		220 °C 48 h	30−50	47
0.225	0.375	0.125	100	1 N 13	7.8 → 7.1		220 °C 48 h	20−50	14
0.45	0.75	0.25	100	1 N	10.2 → 6.8	1/2	220 °C 48 h	20−40	
$VOSO_4$									
0.407		0.125	heat	1 N	5.3		220 °C 48 h	30−60	32
0.407		0.125		1 N	9→8.3		220 °C 48 h	20−30	

[a] Temperature, amount of NaOH and concentration during preparation of precipitate. [b] The pH after addition of NaOH during preparation of precipitate. The pH after hydrothermal reaction is after the arrow. [c] Amount of precipitate used for hydrothermal reaction among the total precipitate formed. [d] Percentage of VO_2(M) among the total product calculated by comparing the intensity of the strongest XRD lines with that of VO_2(B).

Table 4. Reaction Conditions for the Larger Nanocrystals

V_2O_5 (g)	H_2SO_4 (ml)	$N_2H_4 \cdot H_2O$ (ml)	temp (°C)[a]	NaOH[a]	pH[b]	reaction condition	size (nm)	VO_2(M) (%)[c]
0.45	0.75	0.25		1 g/5 mL	5.9 → 3.2	230 °C 48 h	50−100	52
0.45	0.75	0.25	70	1 g/5 mL	4.3 → 3.2	230 °C 48 h	50−100	54
0.45	0.75	0.25	90	1 g/10 mL	4.1 → 3.2	230 °C 48 h	30−80	46
0.45	0.75	0.25		1 g/5 mL	5.7 → 3.0	230 °C 48 h	50−100	53
$VOSO_4$								
0.407		0.125	85	1 N	5.3	220 °C 48 h	100−200	54
0.407		0.125	100	1 N	9.2 → 6.1	220 °C 48 h	50−200	

[a] Temperature, amount of NaOH, and concentration during preparation of precipitate. [b] The pH after addition of NaOH during preparation of precipitate. The pH after hydrothermal reaction is followed by an arrow. [c] Percentage of VO_2(M) among the total product calculated by comparing the intensity of the strongest XRD lines with that of VO_2(B).

reactions. The XRD peaks correspond to VO_2(M) (JCPDS #43-1051) except those marked by asterisks which correspond to VO_2(B) (JCPDS #31-1438). In general, the product was a mixture of the two phases. The percentage of VO_2(M) to VO_2(B) calculated by comparing the intensities of the strongest XRD peaks are given in Tables 1−4. Samples consisting mostly of asterisk-shaped microcrystals (Figure 1A) were mostly or entirely VO_2(M). The XRD pattern of elongated VO_2(M) microrods (Figure 1B) showed peaks other than (*0kl*) were suppressed when compared to Figure 1A, indicating that the monoclinic *a*-axis is the long (growth) direction of the rods. The VO_2(M) microcrystals were usually mixed with VO_2(B) nanorods. VO_2(M) microcrystals could be separated from VO_2(B) nanowires by brief sonication and decantation, or treatment of the product with dilute H_2SO_4 solution which

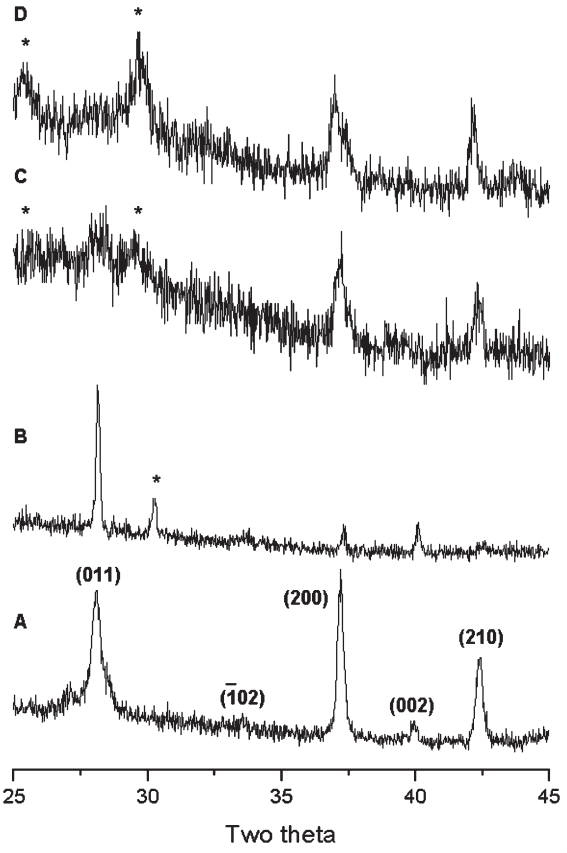

Figure 1. XRD patterns of (A) asterisk-shape microcrystals, (B) microrods, (C) nanocrystals (30−60 nm), and (D) nanocrystals (100−200 nm) showing the peaks of VO_2(M). The peaks corresponding to VO_2(B) are marked by asterisks.

dissolves VO_2(B) nanowires faster than VO_2(M) microcrystals due to the size difference. Both methods could separate the two phases in some degree but not completely. Figures 1C and D are XRD patterns of samples consisting mainly of nanocrystals, showing the mixture of VO_2(M) and VO_2(B) phases and peak broadening due to the nanometer crystal size.

Figure 2 shows SEM and TEM images of VO_2(M) microcrystals. Reaction conditions for producing asterisk-shaped microcrystals and elongated microrods are summarized in Tables 1 and 2, respectively. The asterisk-shaped microcrystals usually consist of six elongated plates with thickness between 50 and 200 nm growing out from the center (Figure 2A and B). The length of the plates varies from 1 to 20 μm and their width from 1 to 5 μm. When the vanadium concentration or pH before the hydrothermal reaction was lower, the result was a mixture of VO_2(M) microrods and VO_2(B) nanorods or nanowires (Figure 2C). Interestingly, VO_2(M) star-shaped six-branched microcrystals and nanorods with very similar morphology have been hydrothermally synthesized from V_2O_5 and excess oxalic acid recently.[34,35] A TEM image of one elongated plate is shown in Figure 2D. A selected area electron diffraction (SAED) pattern of this plate (inset) shows its single crystallinity, and the pattern matches the crystallographic data of VO_2(M) with [010] zone axis and [100] growth direction.

A key motivation for the present work was to synthesize VO_2(M) crystals showing a metal−insulator transition by

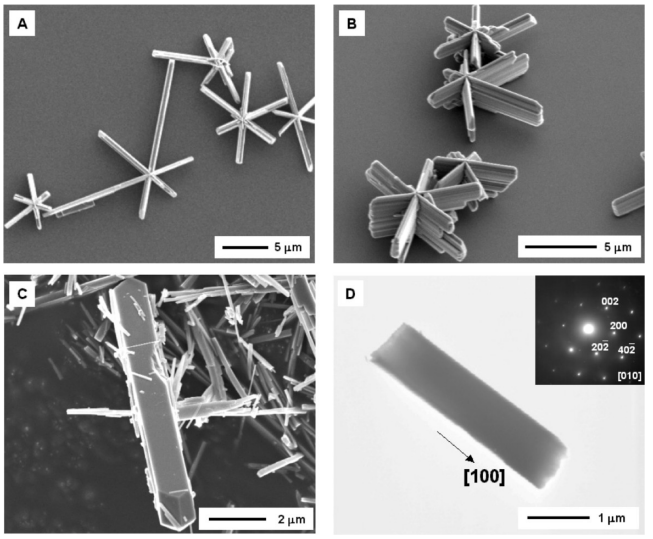

Figure 2. SEM images of (A) long asterisk-shaped VO_2(M) microcrystals, (B) a side view of asterisk-shaped VO_2(M), (C) an elongated VO_2(M) microrod mixed with VO_2(B) nanorods, and (D) TEM image and SAED pattern taken from a branch of asterisk-shaped VO_2(M) microcrystal.

low temperature reaction. We confirmed that an MIT occurs in these microrods by depositing them on a Si/SiO_2 substrate and observing them in an optical microscope while warming, as illustrated in Figure 3. The metallic higher temperature phase appears darker because it absorbs light more strongly than the insulating phase. Each of the larger crystals is seen to darken suddenly at a temperature T_{up} on warming and to lighten suddenly on cooling at a lower temperature T_{down}. Figure 3c shows the values of T_{up} and T_{down} for 30 microrods. The hysteresis ranges from 2 to 5 °C, with T_{up} and T_{down} being on opposite sides of the usual transition temperature of 67 °C consistent with the behavior of nanobeams grown by physical vapor deposition.[16,17] Unfortunately, so far, we have been unable to perform electrical measurements on the nanorods because their adhesion to the SiO_2 substrate is too weak to hold them on while patterning electrodes.

Influence of the Concentration of Vanadium Precursor. The lateral dimensions of VO_2(M) microcrystals depends on the initial vanadium concentration: higher concentrations of vanadium yielded shorter asterisk-shaped crystals, while lower concentrations of vanadium yielded longer asterisk-shaped crystals or elongated rods. We can interpret this as a result of the different levels of supersaturation. At a higher concentration, there might be more chances to form additional seeds on the surface of the preformed crystal, leading to the formation of multiple armed VO_2(M) microcrystals. In contrast, a lower concentration of vanadium would favor the formation of fewer seeds, thus making the crystals grow longer. Subsequently, the ratio of VO_2(M) to VO_2(B) in the short asterisk-shaped microcrystal samples is usually higher than those in the long asterisk-shaped crystal or the elongated rod samples because of the different densities of VO_2(M) seeds. We also note the lower pH value of the solution of short asterisk-shaped crystals after

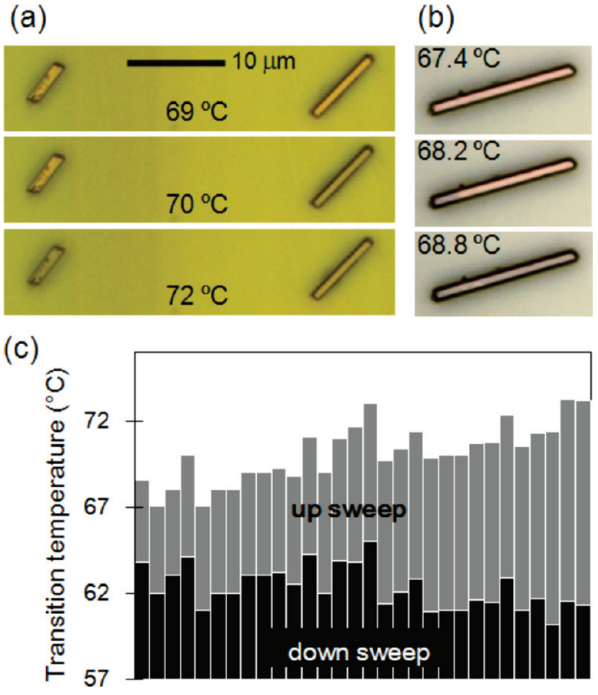

Figure 3. (a and b) Bright-field optical microscope images of VO_2(M) microrods deposited on 1 μm is of SiO_2 on a doped silicon substrate at a series of temperatures on warming. The right microrod in (a) darkens due to the metal−insulator transition between 69 and 70 °C while the left one darkens between 70 and 72 °C. The left portion of the 20 μm rod in b becomes metallic before the right one. (c) Transition temperatures of 30 microrods measured on up and down temperature sweeps, ordered by amount of hysteresis.

hydrothermal reaction, which could have more effectively dissolved the metastable VO_2(B) phase.

Influence of the pH. VO_2 nanocrystals could be synthesized by changing other reaction conditions such as pH, temperature, and concentration of NaOH solution (Figure 4). When the reactant solution pH was higher than 5.5, VO_2 nanocrystals could be obtained instead of microcrystals. Tables 3 and 4 summarize the dependence of nanocrystal size on the reaction conditions. Figures 4A and B show small VO_2 nanocrystals obtained at pH 10, sizes ranging from 20 to 50 nm. The small nanocrystals show a hexagon shape (Figure 4B), but mostly have round corners. This could be due to partial dissolution of nanocrystals in the reaction solution. The nanocrystals usually decomposed to green amorphous precipitate when they were stored in the original reaction solution over a week, accompanied with a pH drop below 5. Figures 4C and D show larger hexagon-shaped VO_2 nanocrystals obtained at pH 8, with sizes ranging from 50 to 200 nm. Electron diffraction from a nanocrystal shows its single crystallinity, and the lattice fringes coincide with those of the microcrystals, confirming the VO_2-(M) phase (Figure 4D). The nanocrystals were usually a mixture of VO_2(M) and VO_2(B), as can be seen by broad XRD peaks of VO_2(B) around 2θ = 26° and 29° (Figure 1C and D). As was calculated from the XRD pattern, the ratio of VO_2(M) to VO_2(B) was relatively lower than that of the VO_2 microcrystals. The mixture of VO_2(M) and VO_2(B) nanocrystals could not be separated.

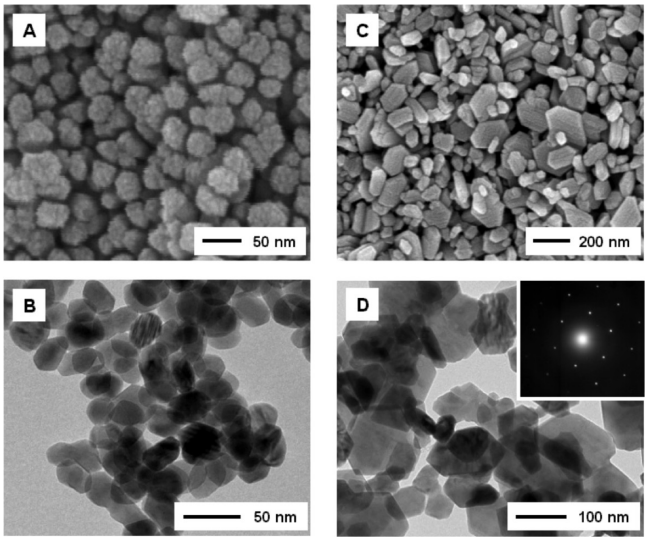

Figure 4. (A) SEM and (B) TEM images of VO_2 nanocrystals (20−50 nm). (C) SEM and (D) TEM of VO_2 nanocrystals (100−200 nm). The inset shows the SAED pattern of a VO_2 nanocrystal.

We do not know the formation mechanism of hexagon shaped nanocrystals, but they are related to VO_2(M) microcrystals in their shape on the basis of the SEM images taken in intergrowth stages (Figure 5). Submicrometer size asterisk-shaped crystals starting to grow branches from hexagon-shaped crystals were observed (Figure 5A and B). Broken branches of asterisk-shaped VO_2(M) microcrystals have pointed ends, thus could be considered as elongated hexagons (Figure 5F). In some cases, a branch of elongated asterisk-shaped microcrystals have penetration twin growth on the same direction with 90° orientation difference (Figure 5C and D). Thickening of the twinned crystal probably forms VO_2(M) microrod crystals (Figure 5E).

Dependence on Reactants. It should be noted that hydrazine was necessary for the formation of VO_2(M). When only NaOH solution was used for the precipitate formation without hydrazine, VO_2(B) nanowires formed exclusively without any VO_2(M) (Figure 6A). We suspect that hydrazine played an important role as a coordinating ligand or reducing agent helping the formation of VO_2-(M). Hydrazine has been described as a structure directing agent for VO_2 hydrate in previous literature.[30] A reducing agent was also used in the recent reports on hydrothermal synthesis of VO_2(M) using V_2O_5 (excess oxalic acid), which suggests a possible role of reducing agents.[34,35]

When small amounts of surfactants such as CTAB, SDS, and PVP or organic ligands such as oxalic acid and sodium citrate were included as additives in the reaction, VO_2(B) selectively formed rather than VO_2(M). This observation indicates that the existence of small amounts of organic molecules in the reaction solution in this system facilitates the formation of VO_2(B).

When the vanadium concentration was lower than 0.1 M or the pH was adjusted lower than 4 while adding NaOH, floating green precipitate sometimes formed after hydrothermal reaction. This product consisted of long

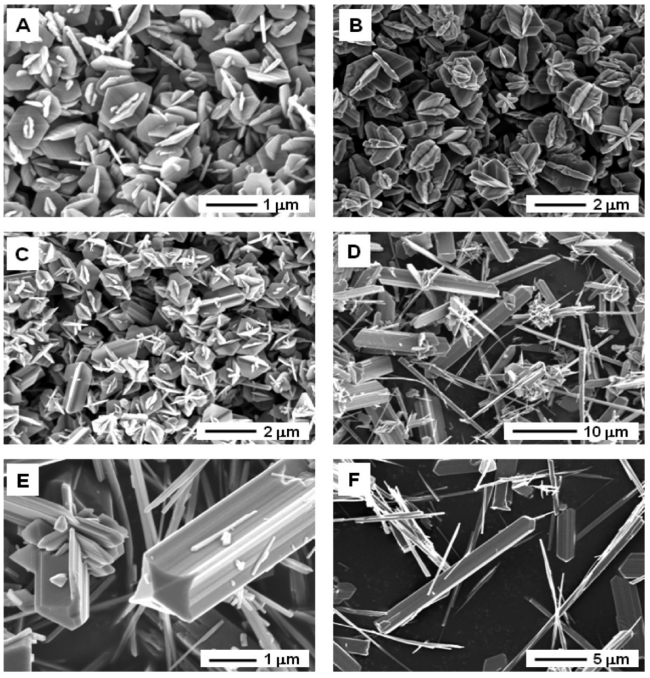

Figure 5. SEM images of VO_2(M) microcrystals in intergrowth stages. (A and B) Hexagon crystals starting to form branches. (C and D) Elongation of the crystal with 90° penetration twinning. (E) Thickening of the twin crystals before microrod formation. (F) Broken branches of VO_2(M) with pointed ends. Nanowires in D−F are VO_2(B) phase.

nanowires of $H_2V_3O_8$, as determined by XRD (JCPDS #28-1433, Figure 6B). The synthesis of $H_2V_3O_8$ has been reported previously.[37] This phase could have been formed due to slight oxidation of the original vanadium precursor.

Fabrication of VO_2(M) Inverse Opals. Figure 7A shows a SEM image of a closely packed PS collidal crystal. The PS spheres form an *fcc* lattice and the (111) surface is parallel to the substrate. The collidal crystal was typically composed of 10−15 layers of PS spheres. Thicker layers could also be obtained by increasing the PS concentration, but the adhesion to the substrate was weaker than for thinner layers so that the packed layers tended to detach from the substrate during VO_2 nanocrystal infiltration. The colloidal crystal had a domain size of tens of micrometers.

Figure 7B shows an SEM image of the PS colloidal crystal infiltrated with VO_2 nanocrystals. The nanocrystals infiltrated the void spaces by capillary force during solvent evaporation. Nanocrystal infiltration into colloidal crystal has been carried out by various methods.[38−43] In our study, ethanol dispersion of VO_2 nanocrystals was used for infiltration. When water was used as a dispersing medium for infiltration instead, VO_2 nanocrystals were

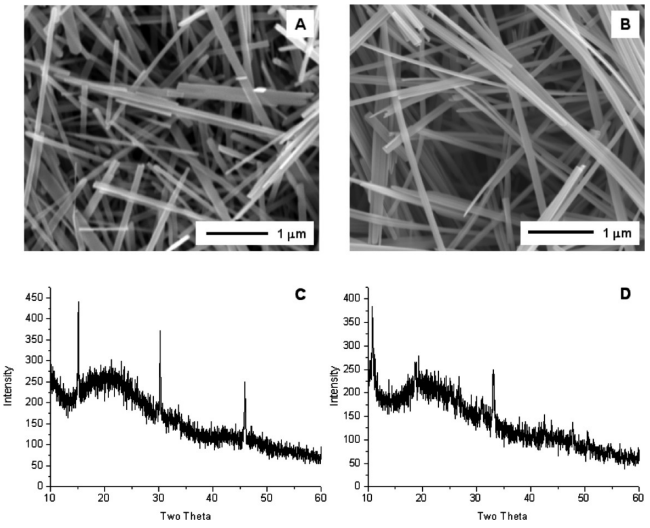

Figure 6. SEM images of (A) VO_2(B) and (B) $H_2V_3O_8$ nanowires. (C and D) XRD patterns of VO_2(B) and $H_2V_3O_8$ nanowires, respectively.

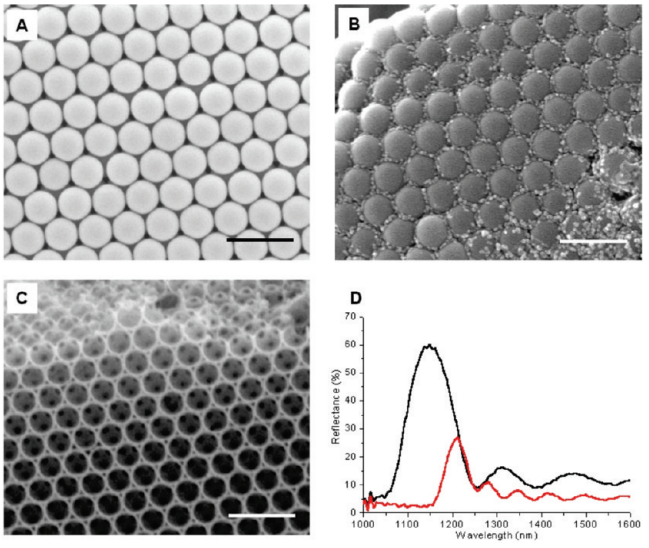

Figure 7. (A) Colloidal crystal of 500 nm PS (B) after infiltration with VO_2 nanocrystals and (C) after calcinations at 500 °C for 2 h with N_2 flowing. (D) NIR reflectance spectra of PS colloidal crystal (black) and after VO_2 infiltration (red). The inverse opal structure (C) did not show any band. The scale bars correspond to 1 μm.

partially oxidized and dissolved to form a green colored solution during the evaporation step, leaving the green deposit infiltrated. By using ethanolic media, hydrolysis and decomposition of VO_2 nanocrystals could be mostly avoided. The concentration of VO_2 was important: low concentration led to incomplete infiltration and high concentration formed an overcoating layer of VO_2 nanocrystals on the colloidal crystal, blocking the photonic crystal structure. The size of the VO_2 crystals was also important. It has been reported that the size of nanocrystals should be ten times smaller than that of the colloid for successful infiltration.[38] We used VO_2 nanocrystals smaller than 50 nm for 500 nm PS colloidal crystal. When larger nanocrystals were used, the nanocrystals did not successfully penetrate the void space but tended to overcoat the surface of the colloidal template.

(37) Li, G.; Chao, K.; Peng, H.; Chen, K.; Zhang, Z. *Inorg. Chem.* **2007**, *46*, 5787.
(38) Gates, B.; Xia, Y. *Adv. Mater.* **2001**, *13*, 1605.
(39) Blanford, C. F.; Yan, H.; Schroden, R. C.; Al-Daous, M.; Stein, A. *Adv. Mater.* **2001**, *13*, 401.
(40) Vlasov, Y. A.; Yao, N.; Norris, D. J. *Adv. Mater.* **1999**, *11*, 165.
(41) Tan, Y.; Qian, W. P.; Ding, S. H.; Wang, Y. *Chem. Mater.* **2006**, *18*, 3385.
(42) Wang, D. Y.; Li, J. S.; Chan, C. T.; Sagueirino-Maceira, V.; Liz-Marzan, L. M.; Romanov, S.; Caruso, F. *Small* **2005**, *1*, 122.
(43) Jiang, P.; Cizeron, J.; Bertone, J. F.; Colvin, V. L. *J. Am. Chem. Soc.* **1999**, *121*, 7957.

Figure 7C shows an SEM image of the inverse opal after calcination. Before calcination, infiltrated VO_2 nanocrystals are usually a mixture of VO_2(M) and VO_2-(B) with an approximately 1:1 ratio. Calcination was carried out in N_2 atmosphere to prevent oxidation of VO_2 and conversion of VO_2(B) nanocrystals into VO_2-(M).[26−31] When calcination was carried out in air, VO_2 converted to yellow V_2O_5. The SEM image shows that the PS template was successfully removed by calcination and the inverse opal VO_2 structure remained. As can be seen in the SEM image, shrinkage of the structure was observed compared to the PS colloidal crystal, to about 77% of its prior size, due to the contraction of the PS and the inverse opal framework during calcination. EDX analysis was carried out to confirm the composition of the inverse opal. The EDX result showed that significant amount of carbon (19 wt %) was included in the inverse opal structure as well as vanadium (36 wt %) and oxygen. We suggest that carbon moieties could not be completely removed due to entrapment in the pores between the VO_2 nanocrystals.

Figure 7D shows the near IR (NIR) reflection of the PS colloidal crystal before and after infiltration with VO_2 nanocrystals. The PS colloidal crystal shows a strong band at 1150 nm, which is close to 1166 nm calculated based on the size of the PS sphere (500 nm). Calculation of the stop band position is given based on the equation below.[44]

$$\lambda = 2d_{111}\sqrt{0.74{n_1}^2 + 0.26{n_2}^2}$$

Here d_{111} is the lattice spacing between (111) planes ($d_{111} = \sqrt{2/3}D$, where D is the diameter of spheres). The refractive index part of the equation was calculated assuming volume occupancy of 74% by spheres (n_1) and 26% by interstices (n_2) in an *fcc* lattice and using the refractive indices of corresponding materials ($n_{air} = 1$, $n_{PS} = 1.55$, and n_{VO2}[45] $= 2.9$).

After infiltration of VO_2 nanocrystals, the band intensity decreased significantly and the bandgap position shifted to 1212 nm, remained much lower than the calculated value (1625 nm), probably due to the partial filling of VO_2 nanocrystals in void spaces. The calculation predicts that the inverse opal should show a reflection band at 1076 nm considering shrinkage of the spherical volume, but the inverse opal did not show any reflection band after calcination. Although not visible in the SEM image, incomplete infiltration of VO_2 nanocrystals could have resulted in long-range order collapsing in the inverse opal after calcination. Additionally, cracks with a dimension of a few micrometers were observed between the inverse opal domains by SEM due to the total volume shrinkage after calcination. The large cracks and a blackbody absorber such as remnant carbon also might be responsible for the absence of NIR reflection band. In

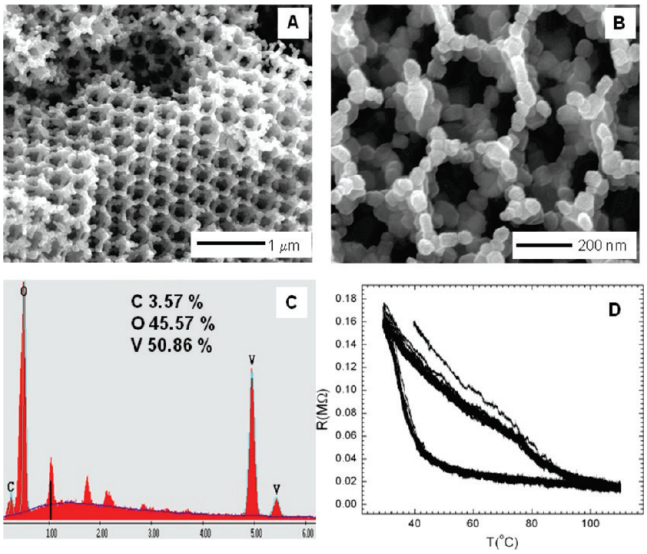

Figure 8. (A and B) VO_2 inverse opal structure fabricated by removing PS template with toluene and subsequent calcination at 500 °C for 2 h. (C) EDX analysis result of the inverse opal. (D) Resistance vs temperature for the inverse opal VO_2 film.

contrast, Pevtsov et al have reported VO_2(M) inverse opal using a chemical bath deposition of V_2O_5 and a reduction in the silica sphere template, which shows a clear stop band shifting on a reversible phase transition.[46−48]

Instead of calcination, toluene was used to dissolve the PS colloidal template to decrease the amount of remnant carbon in the VO_2 inverse opal. The VO_2 inverse opal tended to peel off during the dissolution of the PS with toluene, perhaps due to weaker interconnection between the VO_2 nanoparticles, compared to the calcined sample. To ensure removal of the PS template, the toluene-treated substrate was washed with acetone and calcined at 500 °C for 2 h with N_2 flow. The SEM image of the inverse opal is shown in Figure 8A and B. While a calcined inverse opal structure has a smooth surface, which might be due to the filling of remnant carbon between the VO_2 nanocrystals, toluene-treated inverse opal shows individual nanoparticles interconnected to each other. EDX analysis of the inverse opal shows that the amount of carbon has been significantly reduced compared to the calcined sample (4 wt %) (Figure 8C). To check the phase transition, the resistance of the inverse opal film was measured while changing the temperature (Figure 8D). The resistance of the inverse opal VO_2 film in room temperature was much lower than expected, which might be due to the remnant conducting carbon. Sharp transition could not be observed but a very broad transition with large hysteresis was observed. That could be due to the polycrystalline nature of the inverse opal film and bad interconnectivity between the nanocrystals. A broad hysteresis loop in

(44) Tabata, S.; Isshiki, Y.; Watanabe, M. *J. Electrochem. Soc.* **2008**, *155*, K42.
(45) Cavalleri, A.; Tóth, C.; Siders, C. W.; Squier, J. A.; Ráksi, F.; Forget, P.; Kieffer, J. C. *Phys. Rev. Lett.* **2001**, *87*, 237401.
(46) Golubev, V. G.; Kurdyukov, D. A.; Pevtsov, A. B.; Sel'kin, A. V.; Shadrin, E. B.; Il'inskii, A. V.; Boeyink, R. *Semiconductors* **2002**, *36*, 1043.
(47) Scherbakov, A. V.; Akimov, A. V.; Golubev, V. G.; Kaplyanskii, A. A.; Kurdyukov, D. A.; Meluchev, A. A.; Pevtsov, A. B. *Physica E* **2003**, *17*, 429.
(48) Mazurenko, D. A.; Kerst, R.; Dijkhuis, J. I.; Akimov, A. V.; Golubev, V. G.; Kaplyanskii, A. A.; Kurdyukov, D. A.; Pevtsov, A. B. *Appl. Phys. Lett.* **2005**, *86*, 041114/1.

temperature vs conductivity curve has been previously reported in polycrystalline VO_2 inverse opal also.[46]

Conclusion

Single-crystal VO_2(M) microcrystals and nanocrystals were successfully synthesized by hydrothermal reaction starting from V_2O_5. Varying the reaction conditions such as pH, temperature, and NaOH solution concentration could control the size and shape of the crystals from asterisk-shaped microcrystals to hexagon-shaped nanocrystals. Synthesized VO_2 nanocrystals could infiltrate the PS colloidal crystal, and inverse opal of VO_2 could be fabricated after the removal of the PS template. Although the reaction product was usually a mixture of VO_2(M) and VO_2(B), we believe that low temperature hydrothermal synthesis of VO_2(M) in this study could be further modified to produce phase pure VO_2(M) nanowire which will be important for future applications.

Acknowledgment. J.-H.S. was supported partly by the Korea Research Foundation Grant funded by the Korean Government (MOEHRD, KRF-2006-214-C00042). Geeta Yadav is acknowledged for help in obtaining the phase transition optical images. The research was supported by the U.S. Department of Energy, Office of Basic Energy Sciences, Division of Materials Sciences and Engineering (DE-SC0002197 and DE-FG02-07ER46467), the Army Research Office (48385-PH), Air Force Office of Scientific Research (AFOSR-MURI, FA9550-06-1-0326), and National Science Foundation (DMI-0455994 and DMR-0605159).